ACCSCIENCE PUBLISHING

Explora: Environment and Resource

ORIGINAL RESEARCH ARTICLE

Analysis of thermal effects on sediment grain escape velocity under combined cohesive and viscous forces using the truncated pyramid model

Arijit Dutta[1†] and Sanchayan Mukherjee[2†*]

[1]Department of Mechanical Engineering, Faculty of Engineering, Alipurduar Government Engineering and Management College, Alipurduar, West Bengal, India

[2]Department of Mechanical Engineering, Faculty of Engineering, Kalyani Government Engineering College, Kalyani, West Bengal, India

Abstract

A sediment grain on a riverside is surrounded by similar grains and is subjected to both cohesive and viscous forces. The present study considers the orientation of sediment grains based on the established truncated pyramid model and proposes an expression for the grain's escape velocity. The escape velocity depends strongly on the inter-grain separation gap and temperature for a given water volume entrapped between two neighboring grains. This serves as a key measure of the volumetric erosion rate. A thorough comparative study was conducted, linking the escape velocity values reported in published work—where only cohesive forces were considered—with results obtained when both viscous and cohesive forces were accounted for under varying thermal conditions. Both scenarios were evaluated at a fixed liquid bridge volume and at different separation gaps, while all other parameters were kept constant. The findings revealed that the escape velocity increased relative to that reported in earlier research. In this study, the combined effect of viscous and cohesive forces results in a significant increase in the escape velocity required for a grain, indicating enhanced stability of the riverside compared to cases where only cohesive forces are considered at lower separation times. For the 1st time, temperature dependency is incorporated in the truncated pyramid model. In addition, a one-second threshold was identified, after which viscous forces and temperature no longer significantly affect grain binding.

Keywords: Separation gap; Sediment grain; Cohesive force; Escape velocity; Viscous force; Temperature

†*These authors contributed equally to this work.*

***Corresponding author:**
Sanchayan Mukherjee
(sanchayan.mukherjee@kgec.edu.in)

Citation: Dutta A, Mukherjee S. Analysis of thermal effects on sediment grain escape velocity under combined cohesive and viscous forces using the truncated pyramid model. *Explora Environ Resour*. 2025;2(4):025290055. doi: 10.36922/EER025290055

Received: July 17, 2025

1st revised: September 3, 2025

2nd revised: September 22, 2025

Accepted: September 23, 2025

Published online: October 27, 2025

Copyright: © 2025 Author(s). This is an Open-Access article distributed under the terms of the Creative Commons Attribution License, permitting distribution, and reproduction in any medium, provided the original work is properly cited.

Publisher's Note: AccScience Publishing remains neutral with regard to jurisdictional claims in published maps and institutional affiliations.

1. Introduction

Riverside erosion rates are considerably lower in stable river systems compared to unstable ones. Each grain on a riverside is surrounded by similar grains, held together by gravitational, viscous, and cohesive forces. Gravitational force is the primary driver of sediment grain deposition along a riverside surface, while viscous and cohesive forces between grains act to counter erosion. When the deposition rate of grains is lower than the entrainment rate, erosion occurs. Analyzing erosion mechanisms at the microscale

is challenging due to inherent variability. However, certain analyses can be conducted to examine sediment grain behavior.

Bank erosion can be quantified by determining the escape velocity of the sediment grains. A smaller escape velocity indicates a higher erosion rate. The escape velocity is directly related to the net force exerted by streamflow along the riverside. To date, the literature does not adequately address changes in both viscous and cohesive forces between sediment grains under distinct microscale conditions. In particular, the variation of viscosity with temperature is often overlooked, despite the fact that the temperature of entrapped water cannot remain constant. In this study, escape velocity is calculated by incorporating both viscous and cohesive forces, with viscosity treated as a function of temperature, across varying inter-grain separation gaps and at a fixed liquid bridge volume.

Darby and Thorne[1] analyzed the stability of riversides for shear-driven cohesive banks that fail under planar failure conditions. Urso *et al.*[2] proposed a model to identify the rupture behavior of liquid bridges in grain systems. In addition, several studies[3-5] investigated liquid bridge systems. Yu *et al.*[6] experimentally determined the relationship between porosity and capillary force for mono-size spheres. Groger *et al.*[7] proposed a simulation model to calculate the tensile strain of sediment grains. Hsiau and Yang[8] employed the discrete element method to analyze motion arising from self-diffusion and mixing of cohesive powders in a two-dimensional vibrating granular bed. Rinaldi *et al.*[9] examined the stability of the Sieve riverside by monitoring pore water pressure. Kohonen *et al.*[10] conducted experiments on dynamically deformed wet grains.

Considering equilibrium conditions, Duan[11] analyzed the forces to determine the escape velocity of grains along a riverside. The principal acting forces on a grain are the lift force, the cohesive force between grains, and the submerged weight of the grain. Kotoky *et al.*[12] investigated Brahmaputra riverside erosion. Soulie *et al.*[13] observed the behavior of wet grains under cohesive forces acting at the macro level. Zhang and Li[14] performed a simulation study to observe the dynamic behavior of cohesive soils. Darby and Thorne[15] estimated the tension crack zone in riverside erosion. Mu and Su[16] derived resultant force expressions for liquid bridges between grains. Achite and Oullion[17] investigated grain transport phenomena in watersheds. Cai and Bhushan[18] performed a detailed numerical analysis of viscous and meniscus forces on hydrophobic and hydrophilic surfaces. During this period, several researchers[19,20] developed mathematical models to forecast soil erosion along riversides.

Mukherjee and Mazumdar[21] developed the truncated pyramid model for the arrangement of sediment grains along riversides. They proposed an extensive equation for sediment grain acceleration and escape velocity, demonstrating that this velocity is strongly linked to inter-grain gap and the amount of interstitial water. Al-Shemmeri[22] established a relationship between the dynamic viscosity of water and environmental temperature, indicating that dynamic viscosity exhibits a non-linear relationship with temperature. Chen *et al.*[23] developed a mathematical framework to analyze the delayed failure of unsaturated soil elements subjected to saturation, where the stability conditions of saturated viscous soils were considered. Similarly, Chen and Buscarnera[24] investigated unsaturated porous media through an analytical approach. Zhanlin and Fengxi[25] examined Bingham slurry and explored its diffusion in porous media using seepage theory, with their findings aligning with the transition to a saturated state.

In addition, several researchers[26-28] examined the viscous behavior of unsaturated soils using both experimental and analytical approaches. Biswas *et al.*[29] developed a model to study the rise and fall of water levels associated with planar failure of riverside blocks. An *et al.*[30] evaluated the effect of temperature on the channel gap of electronic devices and identified the optimal gap between the channel and drain metals for thermal performance. Szabo *et al.*[31] discussed water management in detail in their book, where they clearly explained changes in sediment transport parameters, such as shear stress, with variations in discharge. Yang *et al.*[32] developed a theoretical model to explain the dependence of nanofluid viscosity on different physical parameters, primarily temperature. They demonstrated that this model provides more accurate predictive results than many well-known empirical correlations.

In most published studies, the effects of viscous force, cohesive force, or temperature were considered separately. However, in reality, these effects coexist. Therefore, a microscale analysis that combines all of these effects is essential. In this study, the nature of sediment transport under different conditions is analyzed across multiple parameters, and the resulting escape velocity is used to quantify erosion rate.

The viscous force model proposed by Zhang and Li[14] and the cohesive force model suggested by Soulie *et al.*[13] were applied within the truncated pyramid model developed by Mukherjee and Mazumdar.[21] The expression for the variation of dynamic viscosity with temperature, as given by Al-Shemmeri,[22] was incorporated. The present work provides a comprehensive prediction of sediment grain behavior under the combined influence of cohesive and temperature-dependent viscous forces.

2. Methodology

2.1. Force analysis

A liquid bridge formed between two adjacent sediment grains under conditions of low water content leads to cohesion. Cohesive force analysis is based on the assumed geometry of the water bridge. Soulie *et al.*[13] derived expressions for cohesive force in terms of geometric parameters and physical quantities. For a pair of neighboring grains with radii R_1 and R_2, and an inter-grain gap δ, the cohesive force is calculated according to Equation I:

$$F_s = \pi\sigma\sqrt{R_1R_2}\left[c + \exp\left\{a\left(\delta / R\right) + b\right\}\right] \quad (1)$$

where F_s is the cohesive force joining two neighboring grains (N); σ is the surface tension coefficient (N/m); a, b, and c are coefficients considered to be functions of the volume of entrapped water, V (V in nl); $\emptyset$ is the contact angle (radians), and $R = \max(R_1,R_2)$. The expressions for a, b, and c are given as:

$$a = -1.1(V/R^3)^{-0.53} \quad (2)$$

$$b = (-0.148\ln(V/R^3) - 0.96)\,\emptyset^2 - 0.0082\ln(V/R^3) + 0.48 \quad (3)$$

$$c = 0.0018\ln((V)/R^3) + 0.078 \quad (4)$$

At the liquid bridge zone, the viscosity forces acting between two grains can be decomposed into normal and tangential components. Zhang and Li[14] proposed that the vicious force is a function of both physical and geometric parameters. For a pair of side-by-side sediment grains with radii R_1 and R_2, and an inter-grain separation gap $\delta$the tangential and normal viscous forces are expressed as:

$$F_t = 6\pi\eta R^* v_t\,[(8/15)\{\ln(R^*/\delta)\} + 0.9588] \quad (5)$$

$$F_n = 6\pi\eta R^* v_n\,\{R^*/\delta\} \quad (6)$$

where $F_{n\ and}\ F_t$are the normal and tangential viscous force components between a pair of neighboring grains; η is the dynamic viscosity coefficient; v_t is the relative tangential velocity between neighboring grains; v_n is the relative normal velocity between neighboring grains; and R^* is given by:

$$R^* = (R_1R_2)/(R_1 + R_2) \quad (7)$$

In this study, the viscous force model proposed by Zhang and Li[14] and the cohesive force model proposed by Soulie *et al.*[13] were integrated into the truncated pyramid model developed by Mukherjee and Mazumdar.[21] The grain array in this model, along with an enlarged view of a grain pair connected by a liquid bridge, is shown in Figures 1 and 2, respectively.

Here, the tangential velocity between two adjacent grains, v_t, is defined as:

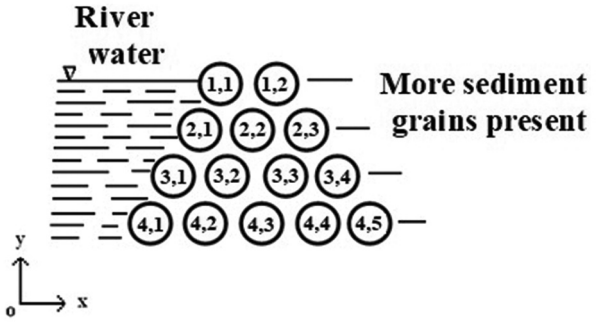

Figure 1. Sediment grain orientation in the truncated pyramid model, showing a trapezium-like arrangement that provides greater stability

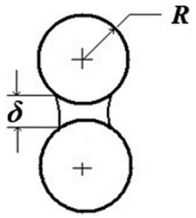

Figure 2. Representation of two neighboring grains connected by a liquid bridge with equal radii (R) and inter-grain separation distance (δ)

$$v_t = \delta/T_s \quad (8)$$

where T_s is the separation time required for a pair of adjacent grains, as proposed by Cai and Bhushan.[18]

The normal velocity between two adjacent grains, v_n, is formulated as:

$$v_n = (R_1 + R_2)/T_s \quad (9)$$

This relation arises from the fact that complete separation occurs when the total distance traversed along the normal direction equals $(R_1 + R_2)$.

Moreover, the dynamic viscosity coefficient, η, is considered to vary with environmental temperature T, as given by Al-Shemmeri:[22]

$$\eta = 2.414x10^{-5}\,x10^{\frac{247.8}{T-140}} \quad (10)$$

When temperature is given in Celsius, Equation 10 is expressed as:

$$\eta = 2.414x10^{-5}\,x10^{\frac{247.8}{T+133}} \quad (11)$$

2.2. Basic framework

Figure 1 depicts the arrangement of grains, while Figure 2 illustrates two neighboring grains. In this arrangement, each grain was placed atop two grains to ensure stability. The riverside configuration depends on grain size, inter-grain gap, and liquid bridge volume. Grains were assumed

to be spherical and materially homogeneous. The surface contact angle was taken as zero, considering pure water in the present analysis. Angles were determined by taking the radii of the three neighboring grains. In the truncated pyramid model, all spherical grains were assumed to have equal grain size (i.e., having equal radii, R). In addition, all grains were considered to be separated by an equal inter-grain distance. The truncated pyramid model exhibits a trapezium-like arrangement for greater stability and was therefore adopted.

2.3. Expression for the escape velocity

Figure 3 illustrates the forces acting on grains e and f. Here, f represents the x-direction coordinate and e represents the y-direction coordinate. F_s, F_t, and F_n indicate cohesive force, viscous tangential force, and viscous normal force between two neighboring grains, respectively. F_G is the weight of the submerged grain. When the equilibrium of a dynamic nature is considered, the minimum acceleration required to detach a grain from the riverside, known as the impending acceleration, can be determined for both the x- and y-components of acceleration. The velocity of the grain corresponding to this minimum acceleration, referred to as the escape velocity, is obtained from the impending acceleration itself. The mass of e, f is given as $4\pi R_{e,f}^3 \rho_s$, assuming each grain is a sphere, where ρ_s is the sediment grain material density.

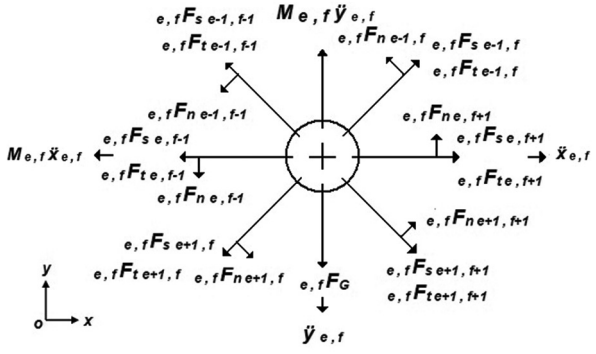

Figure 3. Force diagram of sediment grain (e,f) showing the interactions between the forces and their neighboring grains

The angles between the adjacent grains and the central grain, e, f, expressed in terms of their cosines and based on the radii of the three neighboring grains, are given as (**Equations 12-15** See Page no 6):

The impending acceleration along the x-direction is calculated as (**Equations 16-28** See Page no 6-7):

The impending acceleration along the y-direction is calculated as: (**Equations 29-47** See Page no 7-10):

In addition, g denotes gravitational acceleration and ρ indicates water density.

The resulting impending acceleration of sediment grain e, f is expressed as:

$$f_{e,f} = \left(\ddot{x}_{e,f}^2 + \ddot{y}_{e,f}^2\right)^{0.5} \quad (48)$$

According to Duan,[11] the sediment grain e,f is considered entrained when it is lifted by a gap equal to its diameter. From the law of conservation of linear momentum, the escape velocity of the sediment grain e, f is given by:

$$V_{escape\ e,f} = (2R_{e,f} f_{e,f})^{0.5} \quad (49)$$

The escape velocity is a function of the entrainment rate. For specific cases, volumetric bank erosion may be derived by determining the entrainment rate of grains, the deposition rate of grains, and porosity. According to Duan,[11] from available field data, the entrainment rate of grains, deposition rate of grains, and porosity can be obtained. Considering already established relationships of these parameters with escape velocity, the volumetric erosion rate can be quantified under cohesive and viscous forces.

3. Results and discussion

Mukherjee and Mazumdar[21] derived the escape velocity of grains by considering only cohesive forces at the riverside (f = 1). They assumed all grains had an equal diameter of 0.0008 m. To determine the grain's escape velocity, they considered the following parameters:

(i) Liquid bridge volume, V = 20 nL.
(ii) Surface tension coefficient,σ = 0.073 N/m.
(iii) Contact angle,$\emptyset$ = 0 (assuming pure water for simplicity).
(iv) Water density, ρ = 1,000 kg/m^3.
(v) Grain material density, ρ_s = 2,650 kg/m^3.

Their findings were adopted in the present study to validate the escape velocity using the same input parameters.

Using the above parameters, the dynamic viscosity coefficient η was determined for water at temperatures ranging from 10°C to 40°C, expressed as a function of temperature. In addition, three separation times () were considered: 10^{-7} s, 10^{-4} s, and 1 s.

Tables 1 and 2 summarize the changes in escape velocity with respect to inter-grain separation gap, both for cohesion alone and for the combined effect of viscous and cohesive forces. For the viscous force, the thermal effect on escape velocity at a fixed separation gap was also examined for each separation time and liquid bridge volume.

Figures 4-6 depict the changes in grain escape velocity with varying inter-grain separation gaps, considering either cohesive force alone or the combination of viscous

Table 1. Escape velocity at a separation time of 10^{-7} s for 20 nL liquid bridge volume

Separation gap (m)	Escape velocity due to cohesive force (m/s)	Escape velocity due to cohesive and viscous force (m/s) at different temperatures						
		10°C	15°C	20°C	25°C	30°C	35°C	40°C
0.000145	0.3944	10.2200	9.5539	8.9707	8.4568	8.0012	7.5951	7.2314
0.000150	0.3899	10.0451	9.3905	8.8173	8.3121	7.8643	7.4652	7.1078
0.000155	0.3855	9.8789	9.2351	8.6714	8.1746	7.7342	7.3417	6.9902
0.000160	0.3812	9.7207	9.0872	8.5325	8.0437	7.6103	7.2242	6.8782
0.000165	0.3769	9.5698	8.9462	8.4001	7.9188	7.4923	7.1121	6.7715
0.000170	0.3727	9.4258	8.8116	8.2737	7.7997	7.3796	7.0051	6.6697

Table 2. Escape velocity at a separation time of 10^{-4} s for 20 nL liquid bridge volume

Separation gap (m)	Escape velocity due to cohesive force (m/s)	Escape velocity due to cohesive and viscous force (m/s) for different temperatures						
		10°C	15°C	20°C	25°C	30°C	35°C	40°C
0.000145	0.3944	0.4396	0.4309	0.4242	0.4191	0.4150	0.4118	0.4092
0.000150	0.3899	0.4344	0.4259	0.4194	0.4143	0.4103	0.4072	0.4047
0.000155	0.3855	0.4293	0.4210	0.4146	0.4097	0.4058	0.4027	0.4002
0.000160	0.3812	0.4244	0.4163	0.4100	0.4052	0.4013	0.3983	0.3959
0.000165	0.3769	0.4197	0.4117	0.4056	0.4008	0.3970	0.3940	0.3916
0.000170	0.3727	0.4151	0.4073	0.4012	0.3965	0.3927	0.3898	0.3874

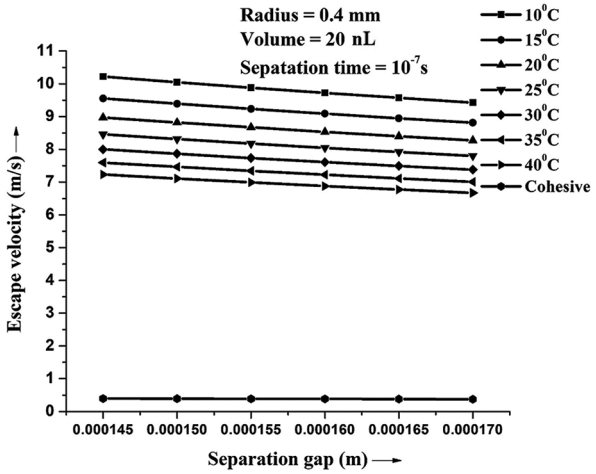

Figure 4. Escape velocity versus inter-grain separation gap at a separation time of 10^{-7} s and 20 nL liquid bridge volume

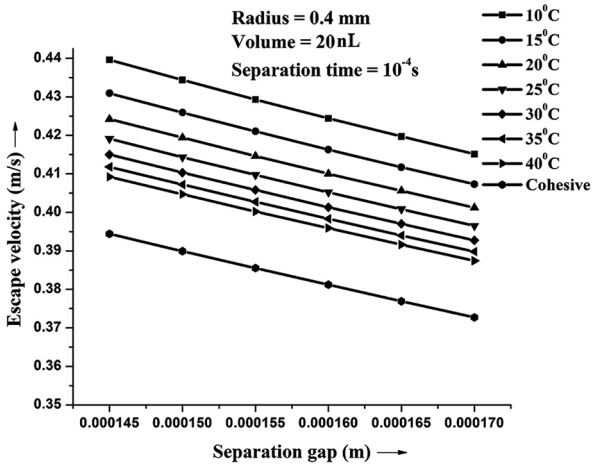

Figure 5. Escape velocity versus inter-grain separation gap at a separation time of 10^{-4} s and 20 nL liquid bridge volume

and cohesive forces, under different temperatures and separation times, for a constant bridge volume of 20 nL.

Figures 4-6 illustrate that the escape velocity requirement decreases as the inter-grain separation gap increases. The results indicate that at larger separation gaps, significantly lower escape velocity is required for the separation of a sediment grain from the bank. In addition, as temperature increases from 10°C to 40°C, the escape velocity decreases at a given separation gap, separation time, and liquid bridge volume. This temperature rise results in a reduction in the dynamic viscosity coefficient and viscous force of the liquid due to the decrease in intermolecular cohesive force.

At a given liquid bridge volume (e.g., 20 nL), the escape velocity requirement considering both viscous and cohesive forces was significantly greater than that considering cohesive force alone at a separation time of 10^{-7} s, as suggested by Cai and Bhushan.[18] The escape velocity decreased with increasing separation time, taken

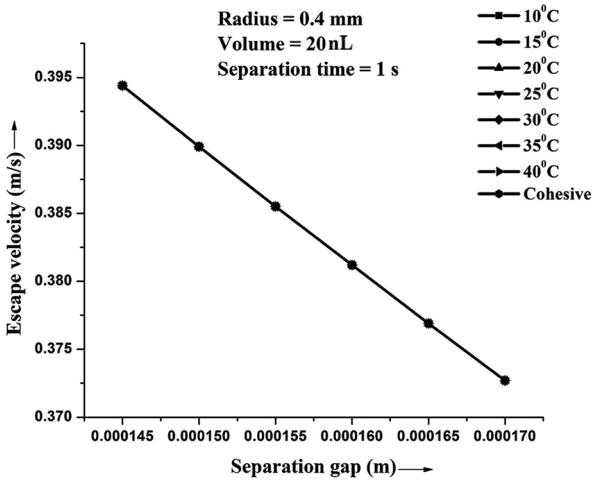

Figure 6. Escape velocity versus inter-grain separation gap at a separation time of 1 s and 20 nL liquid bridge volume

as 10^{-4} s and 1 s, at a fixed separation gap and temperature. Cai and Bhushan[18] demonstrated that the influence of viscosity at a particular liquid bridge persists only for short durations, such as a separation time of 10^{-7} s. Beyond this duration, the impact of viscosity diminishes, and the effect of cohesion increases. It was observed that at a separation time of 1 s, the effect of viscous force vanished, and the escape velocity values were identical to those obtained when considering cohesive force alone, as shown in Figure 6.

With the disappearance of viscous effects at 1 s, the effect of temperature on escape velocity also vanishes. As shown in Figure 6, all temperature-dependent curves overlap with the cohesion-only curve, appearing as a single curve. The escape velocity values were compared with the results reported by Mukherjee and Mazumdar[21] for a 20-nL liquid bridge (Tables 1 and 2). These findings

$$\cos\theta\left(e-1,f:e,f\right)=\left[\left\{\left(R_{e,f}+R_{e-1,f}\right)^2+\left(R_{e,f}+R_{e,f+1}\right)^2-\left(R_{e-1,f}+R_{e,f+1}\right)^2/\left\{2\left(R_{e,f}+R_{e-1,f}\right)\left(R_{e,f}+R_{e,f+1}\right)\right\}\right\}\right] \tag{12}$$

$$\cos\theta\left(e-1,f-1:e,f\right)=\left[\left\{\left(R_{e,f}+R_{e-1,f-1}\right)^2+\left(R_{e,f}+R_{e,f-1}\right)^2-\left(R_{e-1,f-1}+R_{e,f-1}\right)^2/\left\{2\left(R_{e,f}+R_{e-1,f-1}\right)\left(R_{e,f}+R_{e,f-1}\right)\right\}\right\}\right] \tag{13}$$

$$\cos\theta\left(e,f:e+1,f\right)=\left[\left\{\left(R_{e,f}+R_{e,f-1}\right)^2+\left(R_{e,f}+R_{e+1,f}\right)^2-\left(R_{e,f-1}+R_{e+1,f}\right)^2/\left\{2\left(R_{e,f}+R_{e,f-1}\right)\left(R_{e,f}+R_{e+1,f}\right)\right\}\right\}\right] \tag{14}$$

$$\cos\theta\left(e,f:e+1,f+1\right)=\left[\left\{\left(R_{e,f}+R_{e,f+1}\right)^2+\left(R_{e,f}+R_{e+1,f+1}\right)^2-\left(R_{e,f+1}+R_{e+1,f+1}\right)^2/\left\{2\left(R_{e,f}+R_{e,f+1}\right)\left(R_{e,f}+R_{e+1,f+1}\right)\right\}\right\}\right] \tag{15}$$

$$\ddot{x}_{e,f}=\left(3/4\pi R_{e,f}^3\rho_s\right)\left(F_{s1x}+F_{t1x}-F_{n1x}-F_{s2x}-F_{t2x}-F_{n2x}-F_{s3x}-F_{t3x}-F_{s4x}-F_{t4x}+F_{n4x}+F_{s5x}+F_{t5x}+F_{n5x}+F_{s6x}+F_{t6x}\right) \tag{16}$$

$$F_{s1x}=\pi\sigma\sqrt{R_{e,f}R_{e-1,f}}\left[c_{e,f}+\exp\left\{a_{e,f}\left(\delta/R_{e,f}\right)+b_{e,f}\right\}\right]\cos\theta\left(e-1,f:e,f\right) \tag{17}$$

where:

(i) F_{s1x} is the x-direction cohesive force between grains e, f, and $e-1, f$

$$F_{s2x}=\pi\sigma\sqrt{R_{e,f}R_{e-1,f-1}}\left[c_{e,f}+\exp\left\{a_{e,f}\left(\delta/R_{e,f}\right)+b_{e,f}\right\}\right]\cos\theta\left(e-1,f-1:e,f\right) \tag{18}$$

where:

(ii) F_{s2x} is the x-direction cohesive force between grains e, f, and $e-1, f-1$

$$F_{s3x}=\pi\sigma\sqrt{R_{e,f}R_{e,f-1}}\left[c_{e,f}+\exp\left\{a_{e,f}\left(\delta/R_{e,f}\right)+b_{e,f}\right\}\right] \tag{19}$$

where:

(iii) F_{s3x} is the x-direction cohesive force between grains e, f, and $e, f-1$

$$F_{s4x} = \pi\sigma\sqrt{R_{e,f}R_{e+1,f}}\left[c_{e+1,f} + \exp\left\{a_{e+1,f}\left(\delta / R_{e+1,f}\right) + b_{e+1,f}\right\}\right]\cos\theta\left(e,f:e+1,f\right) \quad (20)$$

where:
(iv) F_{s4x} is the x-direction cohesive force between grains e, f, and e+1, f

$$F_{s5x} = \pi\sigma\sqrt{R_{e,f}R_{e+1,f+1}}\left[c_{e+1,f+1} + \exp\left\{a_{e+1,f+1}\left(\delta / R_{e+1,f+1}\right) + b_{e+1,f+1}\right\}\right]\cos\theta\left(e,f:e+1,f+1\right) \quad (21)$$

where:
(v) F_{s5x} is the x-direction cohesive force between grains e, f, and e+1, f+1

$$F_{s6x} = \pi\sigma\sqrt{R_{e,f}R_{e,f+1}}\left[c_{e,f+1} + \exp\left\{a_{e,f+1}\left(\delta / R_{e,f+1}\right) + b_{e,f+1}\right\}\right] \quad (22)$$

where:
(vi) F_{s6x} is the x-direction cohesive force between grains e, f, and e, f+1

$$F_{t1x} = 6\pi\eta\left\{\left(R_{e,f}R_{e-1,f}\right)/\left(R_{e,f}+R_{e-1,f}\right)\right\}\left(\delta / T_s\right)\left[\left(8/15\right)\left\{\ln\left(\left(R_{e,f}R_{e-1,f}\right)/\delta\left(R_{e,f}+R_{e-1,f}\right)\right)\right\}+0.9588\right]\cos\theta\left(e-1,f:e,f\right) \quad (23)$$

where:
(vii) F_{t1x} is the x-direction tangential viscous force between grains e, f, and e−1, f

$$F_{t2x} = 6\pi\eta\left\{\left(R_{e,f}R_{e-1,f-1}\right)/\left(R_{e,f}+R_{e-1,f-1}\right)\right\}\left(\delta / T_s\right)\left[\left(8/15\right)\left\{\ln\left(\left(R_{e,f}R_{e-1,f-1}\right)/\delta\left(R_{e,f}+R_{e-1,f-1}\right)\right)\right\}+0.9588\right]\cos\theta\left(e-1,f-1:e,f\right) \quad (24)$$

where:
(viii) F_{t2x} is the x-direction tangential viscous force between grains e, f, and e−1, f−1

$$F_{t3x} = 6\pi\eta\left\{\left(R_{e,f}R_{e,f-1}\right)/\left(R_{e,f}+R_{e,f-1}\right)\right\}\left(\delta / T_s\right)\left[\left(8/15\right)\left\{\ln\left(\left(R_{e,f}R_{e,f-1}\right)/\delta\left(R_{e,f}+R_{e,f-1}\right)\right)\right\}+0.9588\right] \quad (25)$$

where:
(ix) F_{t3x} is the x-direction tangential viscous force between grains e, f, and e, f−1

$$F_{t4x} = 6\pi\eta\left\{\left(R_{e,f}R_{e+1,f}\right)/\left(R_{e,f}+R_{e+1,f}\right)\right\}\left(\delta / T_s\right)\left[\left(8/15\right)\left\{\ln\left(\left(R_{e,f}R_{e+1,f}\right)/\delta\left(R_{e,f}+R_{e+1,f}\right)\right)\right\}+0.9588\right]\cos\theta\left(e,f:e+1,f\right) \quad (26)$$

where:
(x) F_{t4x} is the x-direction tangential viscous force between grains e, f, and e+1, f

$$F_{t5x} = 6\pi\eta\left\{\left(R_{e,f}R_{e+1,f+1}\right)/\left(R_{e,f}+R_{e+1,f+1}\right)\right\}\left(\delta / T_s\right)\left[\left(8/15\right)\left\{\ln\left(\left(R_{e,f}R_{e+1,f+1}\right)/\delta\left(R_{e,f}+R_{e+1,f+1}\right)\right)\right\}+0.9588\right]\cos\theta\left(e,f:e+1,f+1\right) \quad (27)$$

where:
(xi) F_{t5x} is the x-direction tangential viscous force between grains e, f, and e+1, f+1

$$F_{t6x} = 6\pi\eta\left\{\left(R_{e,f}R_{e,f+1}\right)/\left(R_{e,f}+R_{e,f+1}\right)\right\}\left(\delta / T_s\right)\left[\left(8/15\right)\left\{\ln\left(\left(R_{e,f}R_{e,f+1}\right)/\delta\left(R_{e,f}+R_{e,f+1}\right)\right)\right\}+0.9588\right] \quad (28)$$

where:
(xii) F_{t6x} is the x-direction tangential viscous force between grains e, f, and e, f+1

$$F_{n1x} = 6\pi\eta\left\{\left(R_{e,f}R_{e-1,f}\right)/\left(R_{e,f}+R_{e-1,f}\right)\right\}^2\left\{\left(R_{e,f}+R_{e-1,f}\right)/\left(T_s\delta\right)\right\}\left[1-\cos\theta\left(e-1,f:e,f\right)\right]^{0.5} \quad (29)$$

where:
(xiii)F_{n1x} is the x-direction normal viscous force between grains $e, f,$ and $e-1, f$

$$F_{n2x} = 6\pi\eta\left\{\left(R_{e,f}R_{e-1,f-1}\right)/\left(R_{e,f}+R_{e-1,f-1}\right)\right\}^2\left\{\left(R_{e,f}+R_{e-1,f-1}\right)/\left(T_s\delta\right)\right\}\left[1-\cos\theta\left(e-1,f-1:e,f\right)\right]^{0.5} \quad (30)$$

where:
(xiv)F_{n2x} is the x-direction normal viscous force between grains $e, f,$ and $e-1, f-1$

$$F_{n4x} = 6\pi\eta\left\{\left(R_{e,f}R_{e+1,f}\right)/\left(R_{e,f}+R_{e+1,f}\right)\right\}^2\left\{\left(R_{e,f}+R_{e+1,f}\right)/\left(T_s\delta\right)\right\}\left[1-\cos\theta\left(e,f:e+1,f\right)\right]^{0.5} \quad (31)$$

where:
(xv) F_{n4x} is the x-direction normal viscous force between grains $e, f,$ and $e+1, f$

$$F_{n5x} = 6\pi\eta\left\{\left(R_{e,f}R_{e+1,f+1}\right)/\left(R_{e,f}+R_{e+1,f+1}\right)\right\}^2\left\{\left(R_{e,f}+R_{e+1,f+1}\right)/\left(T_s\delta\right)\right\}\left[1-\cos\theta\left(e,f:e+1,f+1\right)\right]^{0.5} \quad (32)$$

where:
(xvi)F_{n5x} is the x-direction normal viscous force between grains $e, f,$ and $e+1, f+1$

$$\ddot{y}_{e,f} = \left(¾\pi R_{e,f}^3\,\rho_s\right)\left(-F_{s1y}-F_{t1y}-F_{n1y}-F_{s2y}-F_{t2y}+F_{n2y}+F_{n3y}+F_{s4y}+F_{t4y}+F_{n4y}+F_{s5y}+F_{t5y}-F_{n5y}-F_{n6y}\right)+g\left(1-\rho/\rho_s\right) \quad (33)$$

where:
The impending acceleration along the y-direction is calculated as

$$F_{s1y} = \pi\sigma\sqrt{R_{e,f}R_{e-1,f}}\left[c_{e,f}+\exp\left\{a_{e,f}\left(\delta/R_{e,f}\right)+b_{e,f}\right\}\right]\left[1-\cos\theta\left(e-1,f:e,f\right)\right]^{0.5} \quad (34)$$

where:
(i) F_{s1y} is the y-direction cohesive force between grains $e, f,$ and $e-1, f$

$$F_{s2y} = \pi\sigma\sqrt{R_{e,f}R_{e-1,f-1}}\left[c_{e,f}+\exp\left\{a_{e,f}\left(\delta/R_{e,f}\right)+b_{e,f}\right\}\right]\left[1-\cos\theta\left(e-1,f-1:e,f\right)\right]^{0.5} \quad (35)$$

where:
(ii) F_{s2y} is the y-direction cohesive force between grains $e, f,$ and $e-1, f-1$

$$F_{s4y} = \pi\sigma\sqrt{R_{e,f}R_{e+1,f}}\left[c_{e+1,f}+\exp\left\{a_{e+1,f}\left(\delta/R_{e+1,f}\right)+b_{e+1,f}\right\}\right]\left[1-\cos\theta\left(e,f:e+1,f\right)\right]^{0.5} \quad (36)$$

where:
(iii) F_{s4y} is the y-direction cohesive force between grains $e, f,$ and $e+1, f$

$$F_{s5y} = \pi\sigma\sqrt{R_{e,f}R_{e+1,f+1}}\left[c_{e+1,f+1}+\exp\left\{a_{e+1,f+1}\left(\delta/R_{e+1,f+1}\right)+b_{e+1,f+1}\right\}\right]\left[1-\cos\theta\left(e,f:e+1,f+1\right)\right]^{0.5} \quad (37)$$

where:
(iv) F_{s5y} is the y-direction cohesive force between grains $e, f,$ and $e+1, f+1$

$$F_{t1y}=6\pi\eta\left\{\left(R_{e,f}R_{e-1,f}\right)/\left(R_{e,f}+R_{e-1,f}\right)\right\}\left(\delta/T_s\right)\left[\left(8/15\right)\left\{\ln\left(\left(R_{e,f}R_{e-1,f}\right)/\delta\left(R_{e,f}+R_{e-1,f}\right)\right)\right\}+0.9588\right]\left[1-\cos\theta\left(e-1,f:e,f\right)\right]^{0.5} \tag{38}$$

where:
(v) F_{t1y} is the y-direction tangential viscous force between grains $e, f,$ and $e-1, f$

$$F_{t2y}=6\pi\eta\left\{\left(R_{e,f}R_{e-1,f-1}\right)/\left(R_{e,f}+R_{e-1,f-1}\right)\right\}\left(\delta/T_s\right)\left[\left(8/15\right)\left\{\ln\left(\left(R_{e,f}R_{e-1,f-1}\right)/\delta\left(R_{e,f}+R_{e-1,f-1}\right)\right)\right\}+0.9588\right]\left[1-\cos\theta\left(e-1,f-1:e,f\right)\right]^{0.5} \tag{39}$$

where:
(vi) F_{t2y} is the y-direction tangential viscous force between grains $e, f,$ and $e-1, f-1$

$$F_{t4y}=6\pi\eta\left\{\left(R_{e,f}R_{e+1,f}\right)/\left(R_{e,f}+R_{e+1,f}\right)\right\}\left(\delta/T_s\right)\left[\left(8/15\right)\left\{\ln\left(\left(R_{e,f}R_{e+1,f}\right)/\delta\left(R_{e,f}+R_{e+1,f}\right)\right)\right\}+0.9588\right]\left[1-\cos\theta\left(e,f:e+1,f\right)\right]^{0.5} \tag{40}$$

where:
(vii) F_{t4y} is the y-direction tangential viscous force between grains $e, f,$ and $e+1, f$

$$F_{t5y}=6\pi\eta\left\{\left(R_{e,f}R_{e+1,f+1}\right)/\left(R_{e,f}+R_{e+1,f+1}\right)\right\}\left(\delta/T_s\right)\left[\left(8/15\right)\left\{\ln\left(\left(R_{e,f}R_{e+1,f+1}\right)/\delta\left(R_{e,f}+R_{e+1,f+1}\right)\right)\right\}+0.9588\right]\left[1-\cos\theta\left(e,f:e+1,f+1\right)\right]^{0.5} \tag{41}$$

where:
(viii) F_{t5y} is the y-direction tangential viscous force between grains $e, f,$ and $e+1, f+1$

$$F_{n1y}=6\pi\eta\left\{\left(R_{e,f}R_{e-1,f}\right)/\left(R_{e,f}+R_{e-1,f}\right)\right\}^2\left\{\left(R_{e,f}+R_{e-1,f}\right)/\left(T_s\delta\right)\right\}\cos\theta\left(e-1,f:e,f\right) \tag{42}$$

where:
(ix) F_{n1y} is the y-direction normal viscous force between grains $e, f,$ and $e-1, f$

$$F_{n2y}=6\pi\eta\left\{\left(R_{e,f}R_{e-1,f-1}\right)/\left(R_{e,f}+R_{e-1,f-1}\right)\right\}^2\left\{\left(R_{e,f}+R_{e-1,f-1}\right)/\left(T_s\delta\right)\right\}\cos\theta\left(e-1,f-1:e,f\right) \tag{43}$$

where:
(x) F_{n2y} is the y-direction normal viscous force between grains $e, f,$ and $e-1, f-1$

$$F_{n3y}=6\pi\eta\left\{\left(R_{e,f}R_{e,f-1}\right)/\left(R_{e,f}+R_{e,f-1}\right)\right\}^2\left\{\left(R_{e,f}+R_{e,f-1}\right)/\left(T_s\delta\right)\right\} \tag{44}$$

where:
(xi) F_{n3y} is the y-direction normal viscous force between grains $e, f,$ and $e, f-1$

$$F_{n4y}=6\pi\eta\left\{\left(R_{e,f}R_{e+1,f}\right)/\left(R_{e,f}+R_{e+1,f}\right)\right\}^2\left\{\left(R_{e,f}+R_{e+1,f}\right)/\left(T_s\delta\right)\right\}\cos\theta\left(e,f:e+1,f\right) \tag{45}$$

where:
(xii) F_{n4y} is the y-direction normal viscous force between grains $e, f,$ and $e+1, f$

$$F_{n5y}=6\pi\eta\left\{\left(R_{e,f}R_{e+1,f+1}\right)/\left(R_{e,f}+R_{e+1,f+1}\right)\right\}^2\left\{\left(R_{e,f}+R_{e+1,f+1}\right)/\left(T_s\delta\right)\right\}\cos\theta\left(e,f:e+1,f+1\right) \tag{46}$$

where:
(xiii) F_{n5y} is the y-direction normal viscous force between grains $e, f,$ and $e+1, f+1$

$$F_{n6y} = 6\pi\eta\left\{\left(R_{e,f}R_{e,f+1}\right)/\left(R_{e,f}+R_{e,f+1}\right)\right\}^2\left\{\left(R_{e,f}+R_{e,f+1}\right)/\left(T_s\delta\right)\right\} \quad (47)$$

where:
(xiv) F_{n6y} is the y-direction normal viscous force between grains e, f, and e, f+1

All notations used in the text are listed under Appendix.

highlight that a threshold separation time of 1 s exists, beyond which the effect of viscosity becomes negligible and cohesion prevails.

4. Conclusion

Along the riverside, the gap between sediment grains varies depending on local conditions. Thus, a general approach proves highly useful. The inbuilt flexibility of the truncated pyramid model allows for the integration of multiple degrees of freedom, such as sediment grain dimensions, inter-grain separation gaps, geometrical arrays of sediment grains, separation times, and environmental temperatures. Most published studies have focused on either viscous force or cohesive force. In this study, the combined effects of both viscous and cohesive forces, along with thermal variation, were considered and thoroughly investigated. The main findings are as follows:

(i) The grain escape velocity along the riverside decreases, making the bank more vulnerable, as the inter-grain separation gap increases.
(ii) The combined effect of viscous and cohesive forces results in a significant increase in the escape velocity requirement of a grain, indicating greater riverside stability compared to conditions where only cohesion is considered at shorter separation times.
(iii) For a given inter-grain separation gap, separation time, and liquid bridge volume, the escape velocity of a sediment grain decreases with increasing temperature.
(iv) The effect of temperature is valid only up to a threshold separation time of 1 s. Beyond this duration, the effect of viscosity and temperature becomes negligible, and the effect of force of cohesion prevails.

The present study investigated sediment grain behavior in different microscale cases. Predicting the velocity requirement of a sediment grain with temperature for a limiting separation time, considering both viscous and cohesive effects, is essential for practical applications. In addition, the temperature of water in soil varies instead of remaining constant. Based on the analysis, the behavior of sediment grains across varying conditions can be effectively predicted by determining the escape velocity of a grain, which plays a critical role in riverside erosion.

The truncated pyramid model fits well with variations in parameters such as grain size, separation gap between grains, liquid bridge volume, and environmental temperature. However, this model is limited to two-dimensional cases, whereas in reality, all cases are three-dimensional. Therefore, future studies should focus on extending the truncated pyramid model from a two-dimensional to a three-dimensional basis to enable finer data interpretation and more accurate results.

Furthermore, this microscale analysis can be extended to incorporate additional factors such as vegetation effects and the impact of geotextiles, thereby enhancing robustness depending on the data available in real-world situations. Geotextile membranes can function as filters between water and sediment grains, allowing water to pass through while retaining grains, thereby increasing bank stability. Vegetation mitigates erosion through plant root systems that bind soil particles. Thus, integrating geotextile membrane and vegetative root system models into the truncated pyramid model could yield more realistic results.

Acknowledgments

None.

Funding

None.

Conflict of interest

The authors declare that they have no competing interests.

Author contributions

Conceptualization: All authors
Formal analysis: All authors
Investigation: All authors
Methodology: All authors
Visualization: Arijit Dutta
Writing–original draft: All authors
Writing–review & editing: All authors

Ethics approval and consent to participate

Not applicable.

Consent for publication

Not applicable.

Availability of data

All data used here are secondary data taken from published literature, as mentioned in the text.

References

1. Darby SE, Thorne CR. Development and testing of riverbank-stability analysis. *J Hydraul Eng*. 1996;122(8):443-454.

   doi: 10.1061/(ASCE)0733-9429(1996)122:8(443)

2. Urso MED, Lawrence CJ, Adams MJ. A two-dimensional study of the rupture of funicular liquid bridges. *Chem Eng Sci*. 2002;57:677-692.

   doi: 10.1016/S0009-2509(01)00418-3

3. Darby SE, Delbono I. A model of equilibrium bed topography for meander bends with erodible banks. *Earth Surf Process Landf*. 2002;27(10):1057-1085.

   doi: 10.1002/esp.393

4. Rim CS, Gay LW. Estimating soil moisture in small watersheds, using a water balance approach. *Nordic Hydrol*. 2002;33(5):373-390.

   doi: 10.5589/m04-043

5. Simons SJR, Pepin X, Rossetti D. Predicting granule behavior through micro-mechanistic investigations. *Int J Miner Process*. 2003;72:463-475.

   doi: 10.1016/S0301-7516(03)00120-0

6. Yu AB, Feng CL, Zou RP, Yang RY. On the relationship between porosity and inter particle forces. *Powder Technol*. 2003;130:70-76.

   doi: 10.1016/S0032-5910(02)00228-0

7. Groger T, Tuzun U, Heyes DM. Modelling and measuring of cohesion in wet granular materials. *Powder Technol*. 2003;133:203-215.

   doi: 10.1016/S0032-5910(03)00093-7

8. Hsiau SS, Yang SC. Numerical simulation of self-diffusion and mixing in a vibrated granular bed with the cohesive effect of liquid bridges. *Chem Eng Sci*. 2003;58(2):339-351.

   doi: 10.1016/S0009-2509(02)00519-5

9. Rinaldi M, Casagli N, Dapporto S, Gargini A. Monitoring and modelling of pore water pressure changes and riverside stability during flow events. *Earth Surf Process Landf*. 2004;29:237-254.

   doi: 10.1002/esp.1042

10. Kohonen MM, Geromichalos D, Scheel M, Schier C, Herminghaus S. On capillary bridges in wet granular materials. *Physica A Statis Mech Appl*. 2004;339:7-15.

    doi: 10.1016/j.physa.2004.03.047

11. Duan JG. Analytical approach to calculate rate of bank erosion. *J Hydraul Eng*. 2005;131(11):980-989.

    doi: 10.1061/(ASCE)0733-9429(2005)131:11(980)

12. Kotoky P, Bezbaruah D, Baruah J, Sarma JN. Nature of bank erosion along the Brahmaputra River channel, Assam, India. *Curr Sci*. 2005;88(4):634-640.

    doi: 10.1007/BF02989994

13. Soulie F, Youssoufi MSE, Cherblanc F, Saix C. Capillary cohesion and mechanical strength of polydisperse granular materials. *Eur Phys J E Soft Matter*. 2006;21:349-357.

    doi: 10.1140/epje/i2006-10076-2

14. Zhang R, Li J. Simulation on mechanical behavior of cohesive soil by distinct element method. *J Terramech*. 2006;43:303-316.

    doi: 10.1016/j.jterra.2005.05.006

15. Darby SE, Thorne CR. Prediction of tension crack location and riverbank erosion hazards along destabilized channels. *Earth Surf Process Landf*. 2006;19(3):233-245.

    doi: 10.1002/esp.3290190304

16. Mu F, Su X. Analysis of liquid bridge between spherical grains. *China Particuol*. 2007;5:420-424.

    doi: 10.1016/j.cpart.2007.04.006

17. Achite M, Ouillon S. Suspended sediment transport in a semiarid watershed, Wadi Abd, Algeria (1973-1995). *J Hydrol*. 2007;343(3-4):187-202.

    doi: 10.1016/j.jhydrol.2007.06.026

18. Cai S, Bhushan B. Meniscus and viscous forces during separation of hydrophilic and hydrophobic surfaces with liquid-mediated contacts. *Mater Sci Eng*. 2008;61:78-106.

    doi: 10.1016/j.mser.2007.03.003

19. Kisi Ö. River flow forecasting and estimation using different artificial neural network techniques. *Hydrol Res*. 2008;39(1):27-40.

    doi: 10.2166/nh.2008.026

20. Velmurugan A, Swarnam TP, Kumar P. Soil erosion assessment using revised morgan finney model for prioritization of dhanikhari watershed in South Andaman. *Indian J Soil Cons*. 2008;36(3):179-187.

    doi: 10.22541/au.172001663.32097257/v1

21. Mukherjee S, Mazumdar A. Study of effect of the variation of inter-particle distance on the erodibility of a riverbank under cohesion with a new model. *J Hydro Environ Res*. 2010;4:235-242.

    doi: 10.1016/j.jher.2010.01.001

22. Al-Shemmeri T. *Engineering Fluid Mechanics: Fluid Statics*. 1st ed. United States: Ventus Publishing ApS; 2012.

23. Chen Y, Marinelli F, Buscarnera G. Mathematical interpretation of delayed instability in viscous unsaturated soil. *Geotech Lett*. 2020;9(3):165-172.

    doi: 10.1680/jgele.19.00014

24. Chen Y, Buscarnera G. Numerical simulation of unstable suction transients in unsaturated soils: The role of wetting collapse. *Int J Numer Anal Methods Geomech*. 2021;45(11):1569-1587.

doi: 10.1002/nag.3214

25. Zhanlin M, Fengxi Z. Study on diffusion mechanism of viscosity time-varying slurry in unsaturated soil based on displacement effect. *Eur J Environ Civ Eng*. 2023;28(7):1544-1564.

doi: 10.1080/19648189.2023.2263058

26. Cai G, Su Y, Zhou A, Yin F, Shi Y. An elastic-viscoplastic model for time-dependent behavior of unsaturated soils. *Comput Geotech*. 2023;159:105415.

doi: 10.1016/j.compgeo.2023.105415

27. Amarsid L, Awdi A, Fall A, Roux J, Chevoir F. Viscous effects in sheared unsaturated wet granular materials. *J Rheol*. 2024;28(4):523-537.

doi: 10.1122/8.0000824

28. Liangliang W, Zhifei S. Bulk wave manipulation by periodic in-filled barriers in unsaturated soil. *Eng Struct*. 2024;309:118076.

doi: 10.1016/j.engstruct.2024.118076

29. Biswas D, Dutta A, Mukherjee S, Mazumdar A. A new approach to transformation of micro analysis into macro analysis of forces to study the dynamic behaviour of riverbank morphology. *ISH J Hydraul Eng*. 2024;30(3):301-313.

doi: 10.1080/09715010.2024.2317884

30. An DG, Lim UH, Song YS, Kim H, Kim JH. Analysis of thermal effects according to channel and drain contact metal distance. *Case Stud Therm Eng*. 2025;65:105642.

doi: 10.1016/j.csite.2024.105642

31. Szabo J, David L, Loczy D. *Anthropogenic Geomorphology*: *Water management*. 1st ed. Berlin: Springer; 2010.

32. Yang J, Zhao N, Li Z, Sun C. A combined theory model for predicting the viscosity of water-based Newtonian nanofluids containing spherical oxide nanoparticles. *J Therm Anal Calorim*. 2018;135:1311-1321.

doi: 10.1007/s10973-018-7510-6

Appendix

Notations

$a_{e,f}$, $b_{e,f}$, and $c_{e,f}$ coefficients used in the cohesive force equation linking a pair of grains with the bigger grain being e, f

$R_{e,f}$ = Radius of grain e, f, m

δ = Inter-grain separation gap, m

T_S = Separation time, s

T = Temperature, °C

F_{s1x} = x-direction cohesive force linking grains e, f, and $e-1$, f, N

F_{s2x} = x-direction cohesive force linking grains e, f, and $e-1$, $f-1$, N

F_{s3x} = x-direction cohesive force linking grains e, f, and e, $f-1$, N

F_{s4x} = x-direction cohesive force linking grains e, f, and $e+1$, f, N

F_{s5x} = x-direction cohesive force linking grains e,f, and $e+1$,$f+1$, N

F_{s6x} = x-direction cohesive force linking grains e, f, and e, $f+1$, N

F_{s1y} = y-direction cohesive force linking grains e, f, and $e-1$, f, N

F_{s2y} = y-direction cohesive force linking grains e, f, and $e-1$, $f-1$, N

F_{s4y} = y-direction cohesive force linking grains e, f, and $e+1$, f, N

F_{s5y} = y-direction cohesive force linking grains e, f, and $e+1$, $f+1$, N

F_{t1x} = x-direction viscous tangential force linking grains e, f, and $e-1$, f, N

F_{t2x} = x-direction viscous tangential force linking grains e, f, and $e-1$, $f-1$, N

F_{t3x} = x-direction viscous tangential force linking grains e, f, and e, $f-1$, N

F_{t4x} = x-direction viscous tangential force linking grains e, f, and $e+1$, f, N

F_{t5x} = x-direction viscous tangential force linking grains e,f, and $e+1$, $f+1$, N

F_{t6x} = x-direction viscous tangential force linking grains e,f, and e, $f+1$, N

F_{t1y} = y-direction viscous tangential force linking grains e, f, and $e-1$, f, N

F_{t2y} = y-direction viscous tangential force linking grains e, f, and $e-1$, $f-1$, N

F_{t4y} = y-direction viscous tangential force linking grains e, f, and $e+1$, f, N

F_{t5y} = y-direction viscous tangential force linking grains e, f, and $e+1$,$f+1$, N

F_{n1x} = x-direction viscous normal force linking grains e, f, and $e-1$, f, N

F_{n2x} = x-direction viscous normal force linking grains e, f, and $e-1$, $f-1$, N

F_{n4x} = x-direction viscous normal force linking grains e, f, and $e+1$,f, N

F_{n5x} = x-direction viscous normal force linking grains e, f, and $e+1$,$f+1$, N

F_{n1y} = y-direction viscous normal force linking grains e, f, and $e-1$, f, N

F_{n2y} = y-direction viscous normal force linking grains e, f, and $e-1$, $f-1$, N

F_{n3y} = y-direction viscous normal force linking grains e, f, and e, $f-1$, N

F_{n4y} = y-direction viscous normal force linking grains e, f, and $e+1$, f, N

F_{n5y} = y-direction viscous normal force linking grains e, f, and $e+1$, $f+1$, N

F_{n6y} = y-direction viscous normal force linking grains e, f, and e, $f+1$, N

$F_{G\,e,f}$ = Submerged weight of sediment grain e, f, N

$M_{e,f}$ = Mass of sediment grain e, f, kg

$\ddot{x}_{e,f}$ = x-direction impending acceleration of sediment grain e, f, m/s^2

$\ddot{y}_{e,f}$ = y-direction impending acceleration of sediment grain e, f, m/s^2

$f_{e,f}$ = The resulting impending acceleration of sediment grain e, f, m/s^2

$V_{escape\,e,f}$ = Escape velocity of grain e, f from riverside, m/s

g = Gravitational acceleration, m/s^2

ρ = Water density, kg/m^3

ρ_s = Material density of sediment grains, kg/m^3

σ = Coefficient of surface tension, n/m

η = Dynamic viscosity coefficient, pa-s

$\emptyset$ = Contact angle, radians

V = Liquid bridge volume, nL